



**NAVAL
POSTGRADUATE
SCHOOL**

MONTEREY, CALIFORNIA

THESIS

**LASER FREQUENCY STABILIZATION FOR ATOM
INTERFEROMETRY APPLICATIONS**

by

George N. Gilliam

June 2021

Co-Advisors:

Jihane Mimih

Francesco A. Narducci

Second Reader:

Jeffrey G. Lee

Approved for public release. Distribution is unlimited.

THIS PAGE INTENTIONALLY LEFT BLANK

REPORT DOCUMENTATION PAGE			<i>Form Approved OMB No. 0704-0188</i>
Public reporting burden for this collection of information is estimated to average 1 hour per response, including the time for reviewing instruction, searching existing data sources, gathering and maintaining the data needed, and completing and reviewing the collection of information. Send comments regarding this burden estimate or any other aspect of this collection of information, including suggestions for reducing this burden, to Washington headquarters Services, Directorate for Information Operations and Reports, 1215 Jefferson Davis Highway, Suite 1204, Arlington, VA 22202-4302, and to the Office of Management and Budget, Paperwork Reduction Project (0704-0188) Washington, DC 20503.			
1. AGENCY USE ONLY (Leave blank)	2. REPORT DATE June 2021	3. REPORT TYPE AND DATES COVERED Master's thesis	
4. TITLE AND SUBTITLE LASER FREQUENCY STABILIZATION FOR ATOM INTERFEROMETRY APPLICATIONS		5. FUNDING NUMBERS	
6. AUTHOR(S) George N. Gilliam			
7. PERFORMING ORGANIZATION NAME(S) AND ADDRESS(ES) Naval Postgraduate School Monterey, CA 93943-5000		8. PERFORMING ORGANIZATION REPORT NUMBER	
9. SPONSORING / MONITORING AGENCY NAME(S) AND ADDRESS(ES) N/A		10. SPONSORING / MONITORING AGENCY REPORT NUMBER	
11. SUPPLEMENTARY NOTES The views expressed in this thesis are those of the author and do not reflect the official policy or position of the Department of Defense or the U.S. Government.			
12a. DISTRIBUTION / AVAILABILITY STATEMENT Approved for public release. Distribution is unlimited.		12b. DISTRIBUTION CODE A	
13. ABSTRACT (maximum 200 words) <p>Many atomic sensors depend on using a laser with a precisely defined frequency. Unfortunately, most lasers suffer from perturbations in their effective cavity length (which determines the operating frequency of the laser) and active stabilization is required. The atomic interferometry lab at NPS currently uses a laser locking system that has two major problems: The method to determine the desired frequency is not only frequency-sensitive but also intensity-sensitive and the bandwidth of the feedback is too low. The first step in controlling the laser frequency is to find the desired frequency. This value is usually found by taking the midpoint of a transmission peak that is obtained from a doppler-free absorption spectrometer.</p> <p>Currently, this value is the reference frequency for the control system. The current method to determine this reference creates the drawbacks outlined above. To alter the transmission spectrum in a way that eliminates these errors, it is possible to modulate the laser frequency while slowly sweeping across an atomic absorption spectrum. By modulating the signal, the frequency band of the error signal increases which eliminates low frequency noise and thereby improves the accuracy. The modulated signal can then be used to create a new error signal that is used in a feedback system. Once the error signal is defined, it is then used to create a higher speed feedback loop which became limited to 1kHz.</p>			
14. SUBJECT TERMS laser stabilization, atomic sensors, feedback control		15. NUMBER OF PAGES 53	16. PRICE CODE
17. SECURITY CLASSIFICATION OF REPORT Unclassified	18. SECURITY CLASSIFICATION OF THIS PAGE Unclassified	19. SECURITY CLASSIFICATION OF ABSTRACT Unclassified	20. LIMITATION OF ABSTRACT UU

THIS PAGE INTENTIONALLY LEFT BLANK

Approved for public release. Distribution is unlimited.

**LASER FREQUENCY STABILIZATION FOR ATOM INTERFEROMETRY
APPLICATIONS**

George N. Gilliam
Ensign, United States Navy
BS, United States Naval Academy, 2020

Submitted in partial fulfillment of the
requirements for the degree of

MASTER OF SCIENCE IN ELECTRICAL ENGINEERING

from the

**NAVAL POSTGRADUATE SCHOOL
June 2021**

Approved by: Jihane Mimih
Co-Advisor

Francesco A. Narducci
Co-Advisor

Jeffrey G. Lee
Second Reader

Douglas J. Fouts
Chair, Department of Electrical and Computer Engineering

THIS PAGE INTENTIONALLY LEFT BLANK

ABSTRACT

Many atomic sensors depend on using a laser with a precisely defined frequency. Unfortunately, most lasers suffer from perturbations in their effective cavity length (which determines the operating frequency of the laser) and active stabilization is required. The atomic interferometry lab at NPS currently uses a laser locking system that has two major problems: The method to determine the desired frequency is not only frequency-sensitive but also intensity-sensitive and the bandwidth of the feedback is too low. The first step in controlling the laser frequency is to find the desired frequency. This value is usually found by taking the midpoint of a transmission peak that is obtained from a doppler-free absorption spectrometer.

Currently, this value is the reference frequency for the control system. The current method to determine this reference creates the drawbacks outlined above. To alter the transmission spectrum in a way that eliminates these errors, it is possible to modulate the laser frequency while slowly sweeping across an atomic absorption spectrum. By modulating the signal, the frequency band of the error signal increases which eliminates low frequency noise and thereby improves the accuracy. The modulated signal can then be used to create a new error signal that is used in a feedback system. Once the error signal is defined, it is then used to create a higher speed feedback loop which became limited to 1kHz.

THIS PAGE INTENTIONALLY LEFT BLANK

Table of Contents

1	Introduction	1
1.1	Motivation	1
1.2	Status of Research	1
1.3	Thesis Organization	2
1.4	Benefits of Study	3
2	Background and Theory	5
2.1	Laser Interaction	5
2.2	Saturated Absorption Spectroscopy	9
2.3	A Basic Experiment	11
3	Locking Methods	15
3.1	PID Control	15
3.2	Lock-in Amplifier	18
3.3	Increasing the Dither Frequency	24
4	Results	29
5	Conclusion	33
	List of References	35
	Initial Distribution List	37

THIS PAGE INTENTIONALLY LEFT BLANK

List of Figures

Figure 2.1	Diagram of a two-level atom	5
Figure 2.2	Doppler broadening example	7
Figure 2.3	The D2 transition of Rubidium 85	8
Figure 2.4	Different resonance interactions with the laser.	10
Figure 2.5	Diagram of a basic double-pass spectroscopy setup.	12
Figure 2.6	Double pass spectroscopy signal.	13
Figure 3.1	Diagram of a PID controller	15
Figure 3.2	The saturated absorption peaks estimation	17
Figure 3.3	Lock-in amplifier theory	18
Figure 3.4	Diagram of a basic AOM	20
Figure 3.5	Diagram of the advanced lab setup	21
Figure 3.6	Diagram of how the AOM functions.	21
Figure 3.7	Lab setup picture	22
Figure 3.8	Comparison of two signals	23
Figure 3.9	Comparison of the accuracy of the derivative signal	24
Figure 4.1	Unlocked system collected over 4 seconds	29
Figure 4.2	Locked system collected over 4 seconds	30
Figure 4.3	Locked system collected over a day	31

THIS PAGE INTENTIONALLY LEFT BLANK

List of Acronyms and Abbreviations

AOM	Acousto-optic Modulator
AIL	Atomic Interferometry Laboratory
FWHM	Full Width at Half Maximum
GPS	Global Positioning System
INS	Inertial Navigation Systems
NPS	Naval Postgraduate School
PBS	Polarized Beam Splitter
PID	Proportional-Integral-Derivative
RLG	Ring Laser Gyroscope
SNR	Signal-to-Noise Ratio

THIS PAGE INTENTIONALLY LEFT BLANK

Acknowledgments

I would like to thank the U.S. Navy for giving me the opportunity to study at the Naval Postgraduate School (NPS).

I also want to thank Dr. Frank Narducci for his help over the course of the year with research. I appreciate the amount of time he took to help me with the concepts of the lab.

Additionally, I would like to thank Dr. Jeff Lee for his help in the practical applications of the parts in the lab.

THIS PAGE INTENTIONALLY LEFT BLANK

CHAPTER 1:

Introduction

1.1 Motivation

Today almost all navigation relies on the Global Positioning System (GPS) based on a collection of satellites. From the GPS in every smartphone to the systems used by the military aboard ships, satellites allow a user to receive their current position with respect to Earth with a high degree of accuracy. As a result, the military relies heavily on GPS for both land and maritime navigation in a variety of missions. The distance between the satellites and the users of GPS makes it difficult to maintain the integrity of the system from attacks both natural and manmade [1]. As a signal is transmitted from the satellite to the user there is a risk of solar interference, radio interference, and intentional jamming. In order to prepare for an attack on GPS the military must continue to rely on Inertial Navigation Systems (INS) that can determine position based entirely off of inertial measurements.

Inertial navigation systems are made by combining the data from accelerometers and gyroscopes. These two tools measure acceleration and rotation over short periods of time and this data is then integrated to get the desired speed and directional measurements [2]. The measurements can then be combined with an initial position fix, usually gained from GPS, to determine the estimate of the current position. The measurements taken by both the accelerometer and gyroscope are prone to error since neither are an ideal system. While these errors can be minor each time data is collected, since the position estimate is based off an accumulation of previous data and an initial fix, the error grows over time. To combat this, new GPS fixes must be gathered, or the error can continue to grow at least quadratically in the time since the last GPS update until the positional fix is nearly useless for effective navigation [3]. This is particularly important for submarines where they must surface to a detectable depth every time a new fix is required. As a result, there is a desire by the Navy to develop new types of INS to put on naval vessels. Atomic gyroscopes are one option that currently offer orders of magnitude improvement on the current technology in terms of minimizing error and drift over time [4].

1.2 Status of Research

Atomic gyroscopes would be an improvement on the current Ring Laser Gyroscope (RLG) technology that is being used in several military applications today. RLGs function by sending two

beams of light around a closed path and rely on the Sagnac effect to determine the rotation rate [5]. Since these systems rely on the detection of photons, they are burdened by a sensitivity ceiling caused by photon shot noise. Additionally, environmental factors like fluctuating temperatures leading to cavity drifts have proven to introduce additional error over time into RLGs [6]. An atomic gyroscope on the other hand is built off atomic interferometers and relies on particles e.g. rubidium atoms that are far heavier than light particles e.g. photons. The heavier mass affects other errors and leads to greater accuracy within the systems.

Three decades ago, the first experiments proved the viability of atomic sensors and therefore atomic interferometry [7]. Atomic interferometers analyze the motion of atomic waves in the same way that previous interferometers studied light. The rotation and acceleration are detected through the phase difference between two atomic beams. The NPS Atomic Interferometry Laboratory (AIL) has built an interferometer that uses a laser beam to interact with a cloud of atoms. A series of interactions with the atoms causes them accumulate information about the motion in the phase of the atoms. This phase results in a difference in population at the output of the interferometer, which is read out and translated back to information about the motion of the atom.

A source of the error in these experiments arises from the frequency instability of the laser, since the basic function of an interferometer is accomplished through the use of laser pulses. Over the course of time a laser frequency can drift due to cavity length shifting with temperature and other natural causes. For most experiments, the desire is to keep the laser pulse at a frequency where it is capable of exciting the atoms [8]. In order to do so, a scan is taken across a range of frequencies to observe the transitions of the atom. A set point is then taken at the midpoint of a transition peak. The stability of the frequency at that lock point is directly related to the accuracy of the system over a long time. The current system is also susceptible to limited environmental noise causing the system to become unlocked and lose measurements.

1.3 Thesis Organization

Chapter 2 lays the groundwork for saturated absorption spectroscopy starting from the two-level atom and building up to how it was implemented in the lab. Chapter 3 describes the basic control system used to lock the lasers frequency to a fixed frequency. The second part of the chapter explains how the accuracy of the setup is increased by adding a lock-in amplifier and using the same control system. Chapter 4 explores the potential of building a higher frequency feedback system and the consequences of pushing the phase dither to higher frequencies. In Chapter 5 the final control system implemented in the lab is characterized for future use. Finally, Chapter 6 concludes the thesis and describes how the locking theory can be implemented and improved in the

future.

1.4 Benefits of Study

The main goal of a new locking system is to improve the stability of the laser and accuracy of the atomic gyroscope experiments in the NPS AIL lab. This improved stability directly impacts the other experiments taking place in the lab. Additionally, the lab is constructing a larger scale atomic interferometer which would inherently be more sensitive to laser frequency instability and drifts. Ideally, a higher speed feedback loop would be able to offset the introduced error encountered from scaling up the size of the interferometer.

THIS PAGE INTENTIONALLY LEFT BLANK

CHAPTER 2:

Background and Theory

2.1 Laser Interaction

2.1.1 Two-Level Atoms

The basic laser interaction being considered here occurs between a laser and a given two-level atom (an atom with two energy states labeled as the excited and ground state). During the interaction, the atom initially in the ground state absorbs a photon and temporarily enters the excited state. This process is depicted in Figure 2.1. A short time later, the photon is released and the atom returns to the ground state. For the atoms we are interested in (alkali atoms), this process occurs over tens of nanoseconds and results in a photon with approximately the same frequency as the laser at that moment is released. This released photon travels in a random direction away from the atom. As a result, the number of photons in the laser beam has decreased. Due to this action, when the laser frequency is around the natural resonance frequency, ν_0 , of the atom, the transmitted power drops. This resonant frequency is dependent on the difference between atomic energy levels ΔE and Planck's constant h : $\nu_0 = \frac{\Delta E}{h}$ [9].

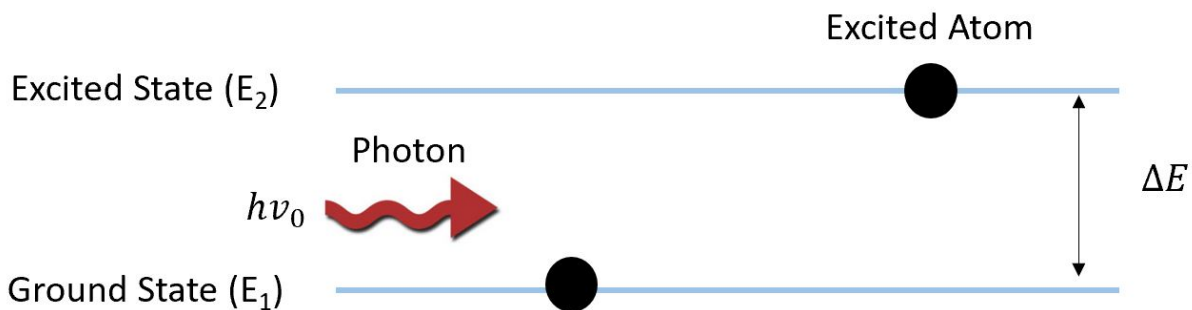


Figure 2.1: An atom at the ground state absorbs a photon traveling at the resonant frequency to temporarily become excited. The photon then is released in a random direction from the excited atom.

For the purposes of our experiment, we are interested in Rubidium, which is a multi-level atom.

The way that a laser interacts with a multi-level atom is similar to that of the two-level atom. The only difference is that the existence of multiple excited states complicates some analysis of the atom.

2.1.2 Uncertainty Broadening

At first, one might think that the spectral profile of a two-level atom would be a delta function in frequency centered at the resonant frequency with no transition probability anywhere else. This assumption would be incorrect due to the Heisenberg Uncertainty Principle which can be used to show that the actual profile takes on a Lorentzian shape with non-zero width [10]. This principle is due to the uncertainty found in both the time measurement Δt and ΔE of the excited state in an atom. The uncertainty is characterized by the relationship $\Delta E \Delta t \geq \hbar$. Here $\hbar = \frac{h}{2\pi}$ where h is the Planck's constant. The resulting linewidth of the spectrum is equal to Δt and is usually reported as the Full Width at Half Maximum (FWHM) points of the spectral line [11].

2.1.3 Doppler Broadening

When using a cell of atoms to study this interaction at a temperature above absolute zero, the atoms all move in different directions as a function of ambient temperature. Atoms moving relative to the laser source will experience a different resonant frequency depending on their individual Doppler shift. This shifted resonance frequency, ν , is given by

$$\nu = \nu_0 + kv = \nu_0 + \frac{2\pi}{\lambda}v, \quad (2.1)$$

where ν_0 is the natural frequency of the atom when $v = 0$, and k is the wave vector of the light with wavelength λ .

For an individual atom moving at a fixed velocity, the spectral shape is maintained with the center of the peak being shifted to a different frequency given by Equation 2.1. These shifts are proportional to the longitudinal velocity of each atom moving in the cell. When one averages over all possible velocities and accounts for the Maxwell-Boltzmann velocity distribution the Doppler broadened line shape is returned. Part (a) of Figure 2.2 shows how some atoms in the cell moving perpendicular to the beam will experience no Doppler shift. The other possibilities are shown in part (b) and (c) where the atom has some relative velocity and shows the change in the transmission spectrum. The result of averaging over all the Doppler shifts can be observed in part (d) of Figure 2.2. For Rubidium at room temperature, the Doppler broadening is a factor of almost 100 times higher than the natural line width [12].

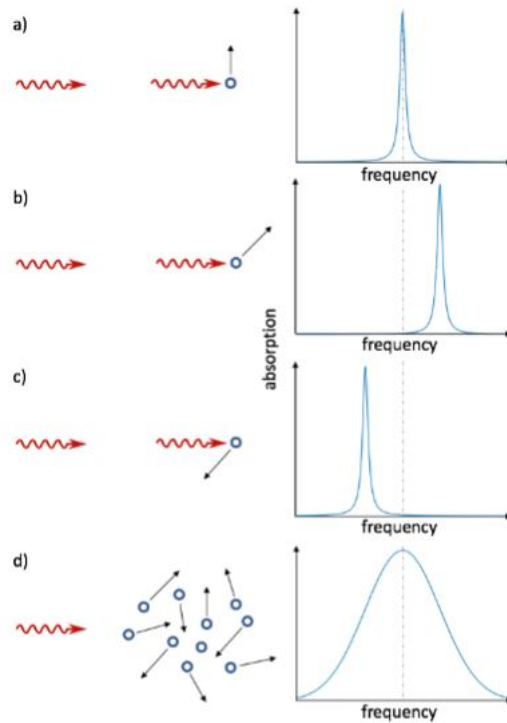


Figure 2.2: The relative motion of each atom in relation to the photon alters the frequency seen by the atom. This shifts the transmission spectrum and over the course of a large sample it broadens the linewidth. Adapted from [13]

If the lab was focused on a two-level atom like hydrogen, this would not be a concern. Since the Maxwell distribution is centered around $v = 0$, the absorption dip in a Doppler-broadened cell is centered around the natural transition frequency for a two-level atom. This means that the actual transition frequency is just the center of the broadened peak. When more energy levels exist, such as in Rubidium that is used in atomic interferometry, this is not the case. Different level spacing and transition strengths result in a Doppler line whose center is shifted with respect to any one transition. As a result, none of the natural frequencies exactly coincide with the peak of the Doppler broadened line. When attempting to drive the correct single energy transition it is vital that we distinguish what transitions are occurring during a scan. Yet the order of magnitude of Doppler broadening is great enough that it masks exact transitions within the larger Doppler broadened image making it difficult to identify specific transitions. Since atomic interferometry relies on transitions occurring in the D2 transition of Rubidium-85, Doppler broadening must be eliminated for the purpose of the lab. The D2 transition that is of interest in the lab is shown in Figure 2.3.

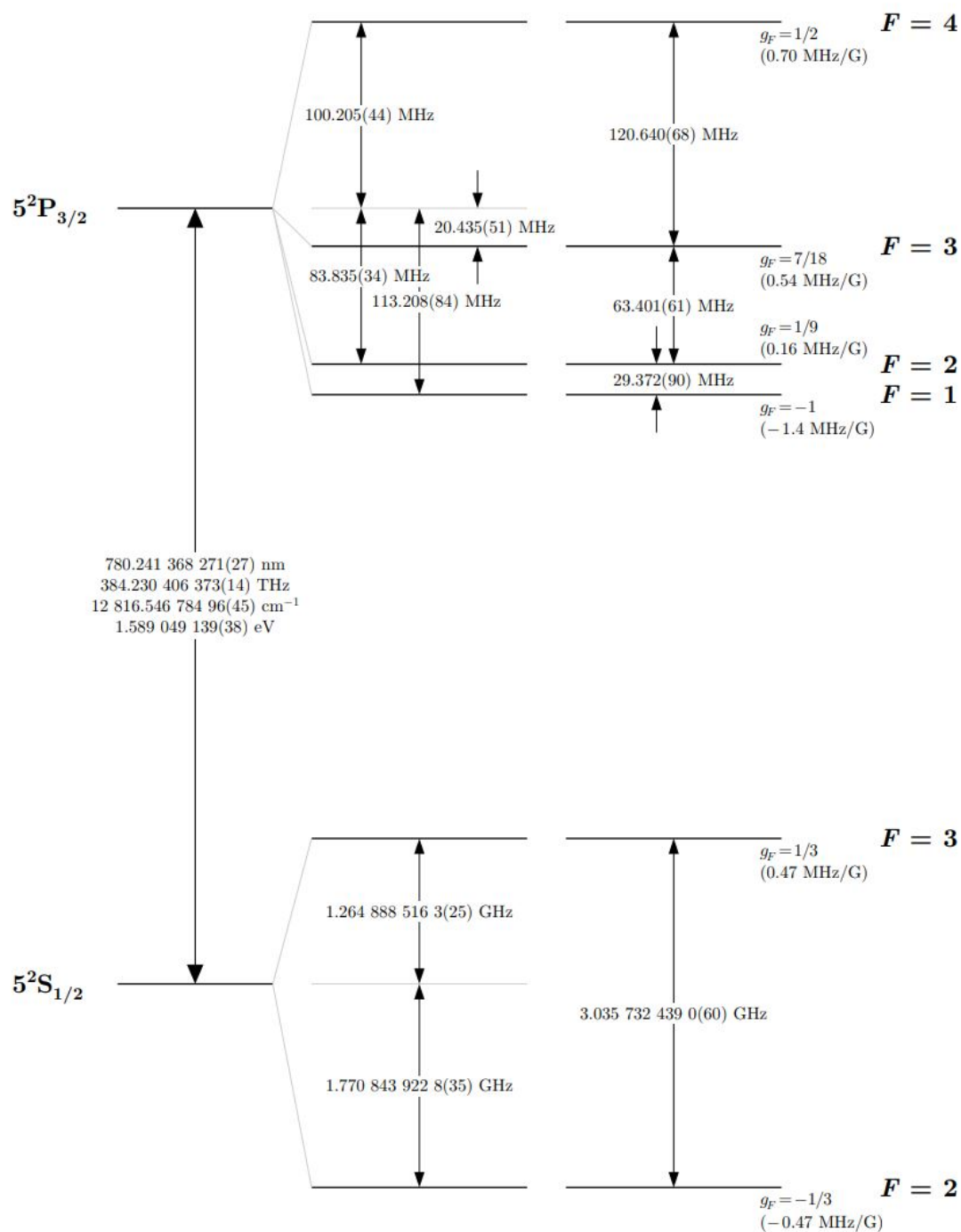


Figure 2.3: A diagram showing the known transition spectrum of the D2 transition for Rubidium 85. Adapted from [14]

2.2 Saturated Absorption Spectroscopy

In order to eliminate Doppler broadening, there are two options: cool the cell of atoms to nearly zero Kelvin or use double pass saturated absorption spectroscopy. The first would be experimentally challenging and the second is quite easy. Therefore, for practical purposes we use a double-pass spectroscopy setup in the lab.

Single-pass spectroscopy is the simplest method of observing laser interactions limited by Doppler broadening by passing a single beam through a cell then measuring the resulting strength of the beam. As the laser frequency is scanned, the measured power dips when atoms are excited and photons are lost to absorption. Doppler broadening impacts these dips and makes it difficult to analyze specific transitions within them.

Double-pass spectroscopy is an improvement on this technique that uses two laser beams. They operate at the same frequency and are counter-propagating. In most instances they can be the same beam that is just retro-reflected. The beams are labeled the pump and probe beam where the pump beam is much stronger relative to the probe. These beams are aligned to overlap spatially resulting in the same atoms being targeted. At most velocities, the atoms will interact with the pump and probe beam at different frequencies due to the Doppler shift. The atom sees the pump beam Doppler shifted in one direction and the probe shifted in the opposite direction. Yet when the atoms are moving at or near perpendicular to the beams, the pump and probe beams will interact with the atom at the same frequency as in Figure 2.4a and b [15]. Since the pump is stronger, it will saturate the atom causing it to not absorb any photons from the probe beam. This process is what eliminates Doppler broadening and allows a transmission closer to the natural frequency of the transition.

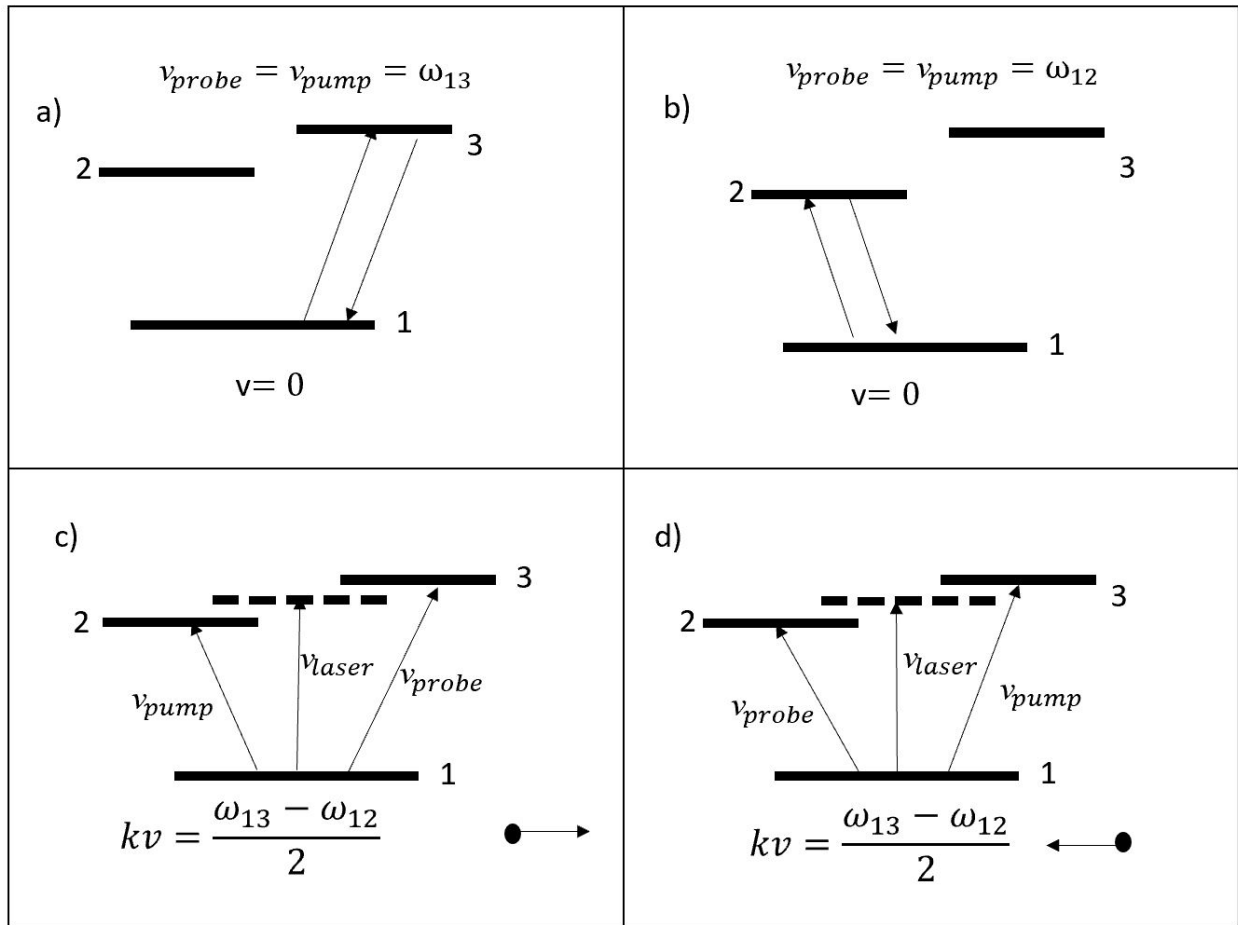


Figure 2.4: These are the four different situations where the pump and probe beam are interacting with the atom at the same frequency. This causes the expected increase in transmission since the pump beam can over saturate the atoms at these four points. The bottom two are the cross-over transitions.

While double-pass spectroscopy is convenient for eliminating Doppler broadening, it does introduce crossover resonance transitions. When considering a double-pass setup, the pump beam reduces the probe beams absorption at the resonant frequencies of an atom by saturating them. This results in peaks at natural frequencies ν_1 and ν_2 . In the transmission spectrum these appear as peaks at the same frequencies. At a frequency halfway between two transitions, $\frac{\nu_1 + \nu_2}{2}$, an atom moving in the same direction as one of the beams can create a situation where the transmission of the probe is increased [15]. For a specific velocity class given by $kv = \frac{\omega_{13} - \omega_{12}}{2}$, the pump can be Doppler shifted down, coinciding with the lower frequency transition. This automatically shifts the probe to be on-resonance with the high frequency transition (Figure 2.4c). The pump robs population from the ground state and hence the probe experiences increased transmission. Figure 2.4d shows the

situation when the atom moves in the other direction. These expected transition frequencies can be observed in Figure 2.3 and are used to interpret collected data.

In some cases, where the transition frequencies are only slightly farther apart than the natural linewidth of an atom, these crossover resonances would mask the true peaks in the spectrum. As a result, this method of eliminating Doppler broadening would introduce a different type of error in the form of artificial peaks instead of Doppler broadening. In the case of Rubidium, the natural linewidth is around 3 MHz and the transition separation is between 30 and 120 MHz. Since the natural linewidth is significantly smaller than the separation, it is possible to distinguish the true and artificial peaks in the transmission spectrum making this a valid method of eliminating Doppler broadening.

2.3 A Basic Experiment

This project began with the construction of a basic saturated absorption experiment. Figure 2.5 highlights the schematic used for the initial experiment. A laser is passed through an optical isolator to prevent any feedback from interfering with the laser. Even at a low level, optical feedback can cause a significant amount of noise. The beam is then passed through a thick optic which reflects two weak beams from the main beam. These two beams are what will eventually be subtracted to create a positive voltage profile for the data collected. The three subsequent beams are all passed through half-wave plates which allow the polarization of each beam to be adjusted. This step is only useful since Polarized Beam Splitter (PBS) are employed to reflect the beams. Finally, the beam that passed through the thick optic, which is stronger than the beams picked off, is reflected back upon one of the other two beams in order to create the desired pump and probe setup. The other beam that was picked off is left alone and used as a zero reference for the subtraction occurring in the photodetector.

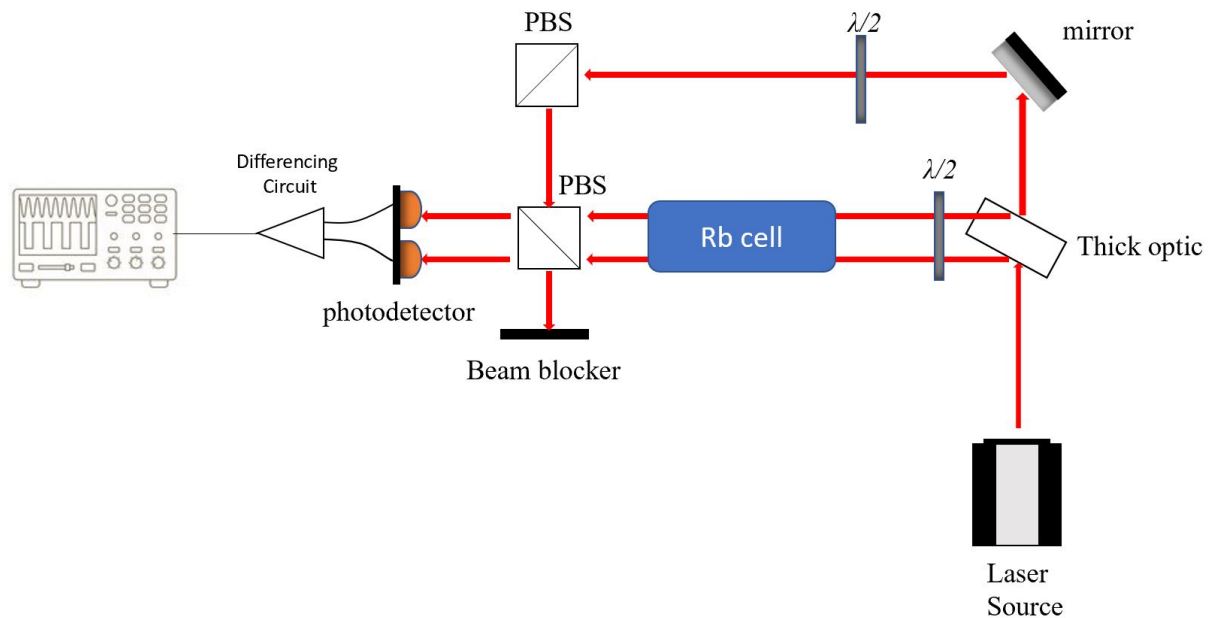


Figure 2.5: The basic double-pass spectroscopy setup used in the lab. This beam on the top of the cell is the one that has the pump and probe beam overlapping with each other.

The results of the basic experiment are seen in Figure 2.6 where the six expected peaks are evident. Since we are mainly concerned with ^{85}Rb , the setup has been tuned to one of the two transitions in that isotope. The initial data collected from an oscilloscope is in the form of voltage versus time. Using the known structure of ^{85}Rb it is possible to convert the time series from the data into a frequency versus voltage plot. Doing so proves that it is possible to control laser frequency through altering the voltage and if the spectrum is collected when taking voltage data, makes it possible to see how a laser is locking not only in voltage terms but in frequency terms. This calculation is demonstrated in Figure 3.2 later on but the original time series is shown in Figure 2.6.

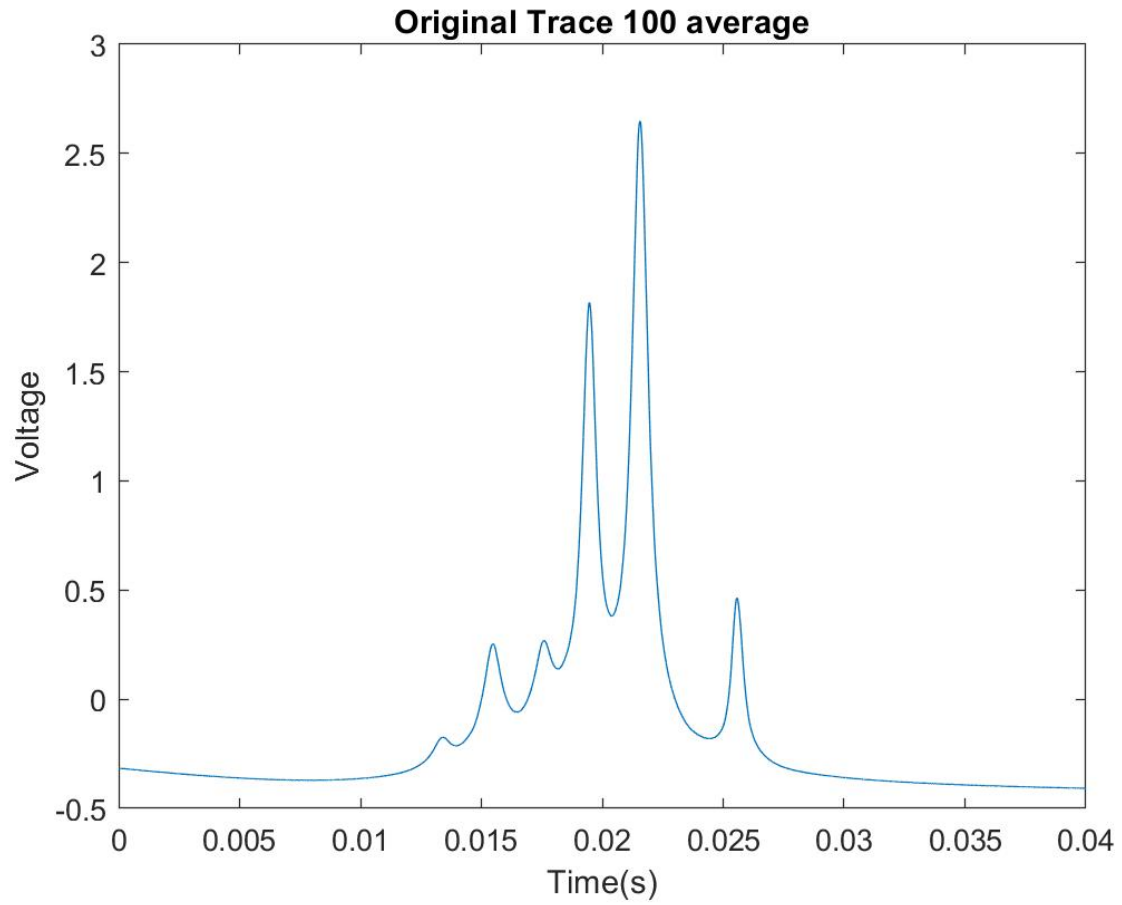


Figure 2.6: This is an averaged form of the signal measured using the setup in Figure 2.5. The six peaks represent the cross-over and true resonance frequencies.

THIS PAGE INTENTIONALLY LEFT BLANK

CHAPTER 3: Locking Methods

A control system is designed to stabilize the output of a system with a constantly changing nature. For the purpose of this lab, we will use a closed loop control system that alters the input signal based upon the error signal. This type of control is needed in order to have the actual output frequency of the laser as close to the desired as possible.

3.1 PID Control

Proportional-Integral-Derivative (PID) control is one of the most used control systems and has been in practice since the early 1900s [16]. It is widely used for its reliability and simplicity in most applications. Per the name it is consisted of three different control circuits which allow for a user to control most errors but also allows a user to manually tune the lock point. It is frequently the case in the lab that the derivative component is eliminated in what is known as PI control, however, this lab uses the derivative control in order to eliminate high frequency disturbances [17].

3.1.1 Theory

The PID controller is created by combining three different elements as observed in Figure 3.1.

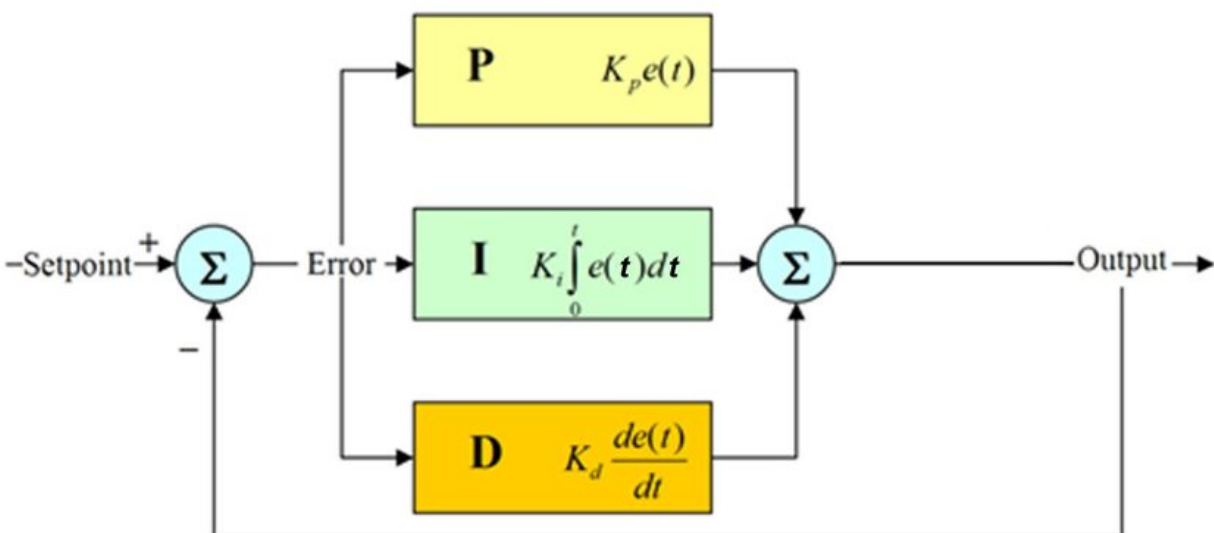


Figure 3.1: This is the basic structure of a PID controller

Proportional Action

The first arm of PID control is the proportional action where the output is simply a constant times the error signal or $K_p * e(t)$ [17]. This piece is designed to focus on controlling the current error in the system. Since the only input term is the current error, it is insufficient at correcting for previous or future errors in the system. The gain of this can be adjusted to alter the strength to which the system responds to initial error. One drawback of proportional control is inevitable steady state error where even though the error signal is minimized between two time terms, it is not equal to the initial reference signal because of the errors in previous iterations. These errors are corrected by the integral action.

Integral Action

In order to combat the steady state error derived from proportional control, it is possible to integrate the error signal. This action corrects for the steady state error since even if the term $e(\Delta t)$ goes to zero for $\Delta t = 0$ [17]. The integral term only does so if there is zero steady state error. As such, the combination of proportional and integral control allows for a system that has zero steady state error and corrects over time. Another way to think about the action of the integral circuit is to think of it as correcting for low frequency drifts.

Derivative Action

The derivative action is intended to correct for future errors by looking at the expected derivative of the error over time. In the ideal this type of control is the same as $K_d \frac{de(t)}{dt}$ [17]. The Taylor expansion of the ideal control demonstrates that this action is based upon the current error and the error at some time difference T_d ahead of the current time. The derivative signal is equivalent to feedback at high frequencies.

3.1.2 Implementation

For the setup in the lab, the output of the saturated absorption is used as the input to the error signal. In order to do this, a voltage offset is applied to the laser controller until there the desired set point on the curve is at zero. An increase in voltage will move the error signal either positively or negatively and allow the system to adjust accordingly. If at any time the value goes over a peak, then the lock is lost since the polarity has changed. The loss of lock possible here is one issue that can be encountered over a long time when the laser either drifts too far over a peak or experiences a shock to the system and is immediately jumped over a peak.

Once a point is locked on, the user can tune the PID gains along with the overall gain of the system to improve the lock. This step can first be accomplished on an oscilloscope by simply looking at

the error signal as a function of time and attempting to minimize the variance seen. At a certain point the changes become indistinguishable and the signal can instead be plugged in to a spectrum analyzer. This allows the user to observe the frequency components of each part of the error on a much more sensitive scale and adjust the PID to minimize the amplitude of the error across a band of frequencies.

3.1.3 Analysis

The data is collected from the oscilloscope in the format of voltage versus time. For this section, we used a code to fit the sum of six Lorentzians of differing amplitudes to the spectrum collected. Figure 3.2 shows the plots superimposed on each other. By making a MATLAB function to approximate the real data, we can convert the voltage data collected when the lock is on into frequency.

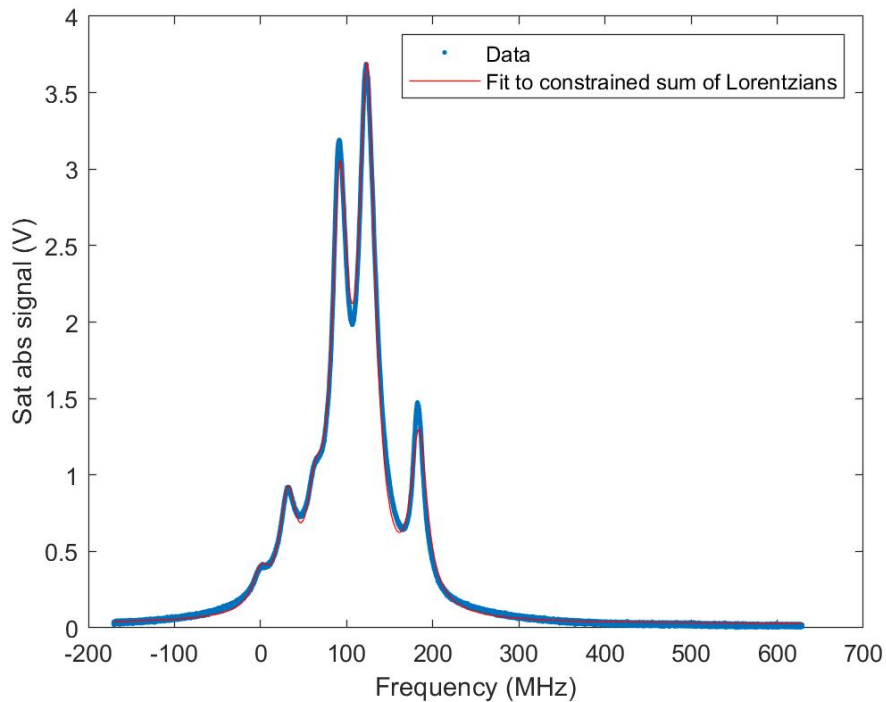


Figure 3.2: This graph overlays the data from the sensors with the estimated Lorentzian that is used in future analysis.

3.2 Lock-in Amplifier

While a PID control system is effective at minimizing an error signal over time, it is only as effective as the signal it is receiving. In the initial setup, the error signal invariably has external noise that makes the system less accurate. One method to eliminate external noise is to implement a lock-in amplifier. The user dithers the desired signal by modulating the laser with a fixed modulation frequency. The lock-in amplifier then detects any signals at the modulation frequency and removes all other components e.g. noise at other frequencies. The resulting signal will minimize external noise but (as we will see) will actually be the derivative of the desired signal. For our purposes this makes the lock point a peak instead of the midpoint on a slope.

3.2.1 Theory

In practical applications noise exists at a variety of frequencies and the signal does as well. The higher frequency components of noise can be eliminated using a low-pass filter, yet this would preserve all low frequency noise along with the signal itself. For the applications concerned in this lab, the signal itself along with a large portion of the noise occur at low-frequencies as in Figure 3.3. This means that a low-pass filter does little to impact the Signal-to-Noise Ratio (SNR) of the overall system and cannot be used to significantly improve the lock. Additionally, using a low-pass filter would slow the feedback loop down and not allow us to control errors at higher frequencies. Instead, if it possible to move the signal to a higher frequency, then there are regions where the SNR would be drastically increased using a band-pass filter.

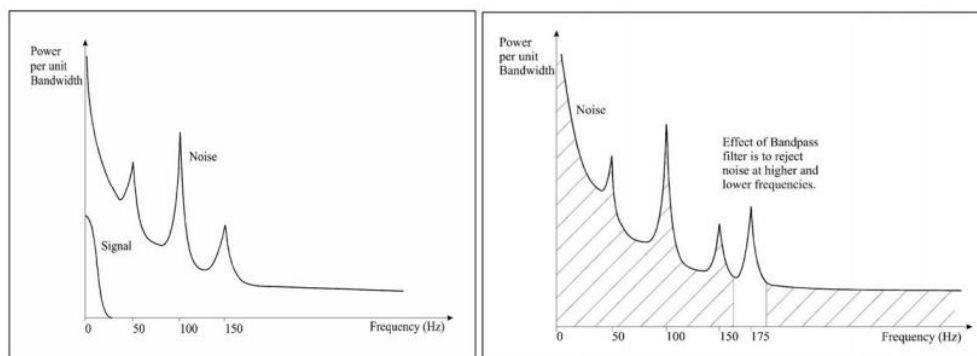


Figure 3.3: The plot on the left shows how a signal at low frequency can be masked by noise how it is not possible to filter out. The right shows what happens when a signal is shifted to higher frequency and how it can be measured with much lower noise. Adapted from [18].

For the purpose of this experiment, we will modulate the frequency of the pump beam or the

detuning. If we take a resonance line from an atomic transition to be a Lorentzian of half width at half maximum to be β , then we can write

$$V_s = \frac{I}{\beta^2 + \delta^2}, \quad (3.1)$$

where V_s is the voltage measured. Then we modulate the detuning where $\delta = \delta_0 + m \cos \Omega t$ and we have

$$\delta^2 = \delta_0^2 + 2\delta_0 m \cos \Omega t, \quad (3.2)$$

and then

$$V_s = \frac{I}{\beta^2 + \delta_0^2 + 2\delta_0 m \cos \Omega t}. \quad (3.3)$$

It is important to note that in the previous step we can rewrite the $\cos^2(\Omega t)$ as a $\cos(2\Omega t)$. Since the lock-in amplifier will ignore frequencies that are not equal to Ω , this term does not contribute to the signal and we will ignore it from here on. Simplifying this we get

$$\frac{I}{\beta^2 + \delta_0^2 + 2\delta_0 m \cos \Omega t} = \frac{I}{(\beta^2 + \delta_0^2) \left[1 + \frac{2\delta_0}{\beta^2 + \delta_0^2} m \cos \Omega t \right]} \approx \frac{I}{\beta^2 + \delta_0^2} - \frac{I}{\beta^2 + \delta_0^2} \frac{2\delta_0}{\beta^2 + \delta_0^2} m \cos \Omega t, \quad (3.4)$$

where we have used a Taylor expansion in the last step. The lock-in amplifier mixes the detected signal with a modulated signal of the same frequency which results in

$$V_s \cos(\Omega t + \phi) = \frac{I}{\beta^2 + \delta_0^2} \cos(\Omega t + \phi) - \frac{I}{\beta^2 + \delta_0^2} \frac{2\delta_0}{\beta^2 + \delta_0^2} m \cos \Omega t \cos(\Omega t + \phi) \quad (3.5)$$

$$= \frac{I \cos(\Omega t + \phi)}{\beta^2 + \delta_0^2} - \frac{I}{(\beta^2 + \delta_0^2)^2} \frac{2\delta_0 m}{2} [\cos \phi + \cos(2\Omega t + \phi)]. \quad (3.6)$$

Note : $\left. \frac{dV_s}{d\delta} \right|_{\delta=\delta_0} = -\frac{2I\delta_0}{(\beta^2 + \delta_0^2)^2}$.

Averaging the right hand side over an appreciable length of time (long compared to a time $\frac{1}{\Omega}$) is the equivalent of the lock-in amplifier time constant element. Only the derivative term survives, leaving

$$V_{filter} = \frac{1}{2} \left. \frac{dV_s}{d\delta} \right|_{\delta=\delta_0} m \cos \phi. \quad (3.7)$$

3.2.2 Implementation

In order to achieve the desired frequency dither in the lab we use an Acousto-optic Modulator (AOM). When a beam is passed through an AOM there is an internal acoustic travelling wave which shifts the initial beam by the acoustic frequency (of order several tens of MHz) as seen in Figure 3.4.

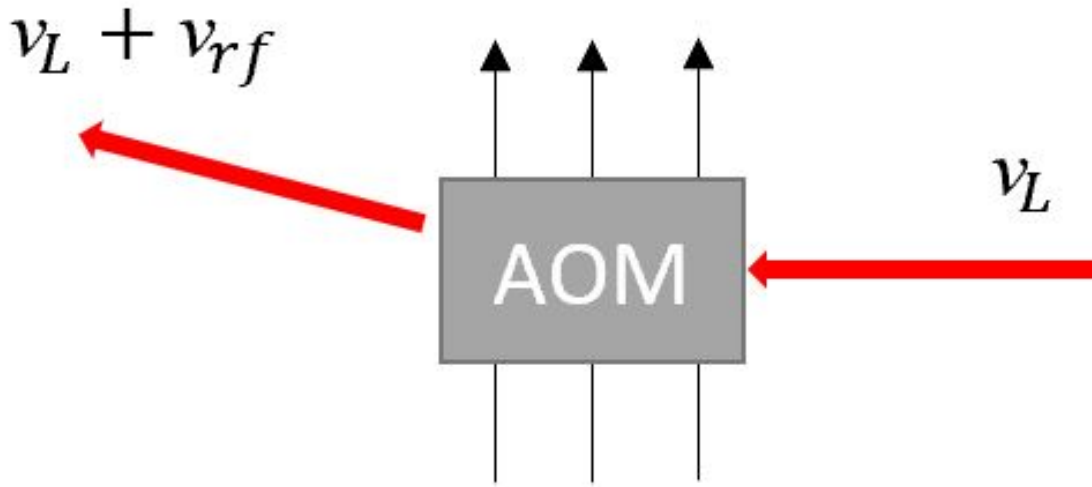


Figure 3.4: This is the diagram of the basic laser interaction when an AOM is used in the lab.

An AOM can be added to the basic saturated absorption setup seen in figure 2.5 to modulate the detuning. Figure 3.5 shows the new schematic where the pump beam has its phase modulated by the AOM. The beam passes through the AOM twice and is aligned so there is a $2\nu_{rf}$ phase shift when the beam is reflected into the original beam. Since the beam passing through the AOM is split in to 3 different beams, the positive, negative, and zero order phase shift, it is important to block the undesirable beams and properly collimate the beam to be used. The direction that the AOM used alters the phase shift is shown in Figure 3.6 and as such the straight beam reflected has the desired frequency shift. Figure 3.7 demonstrates how the diagrams were implemented in the lab.

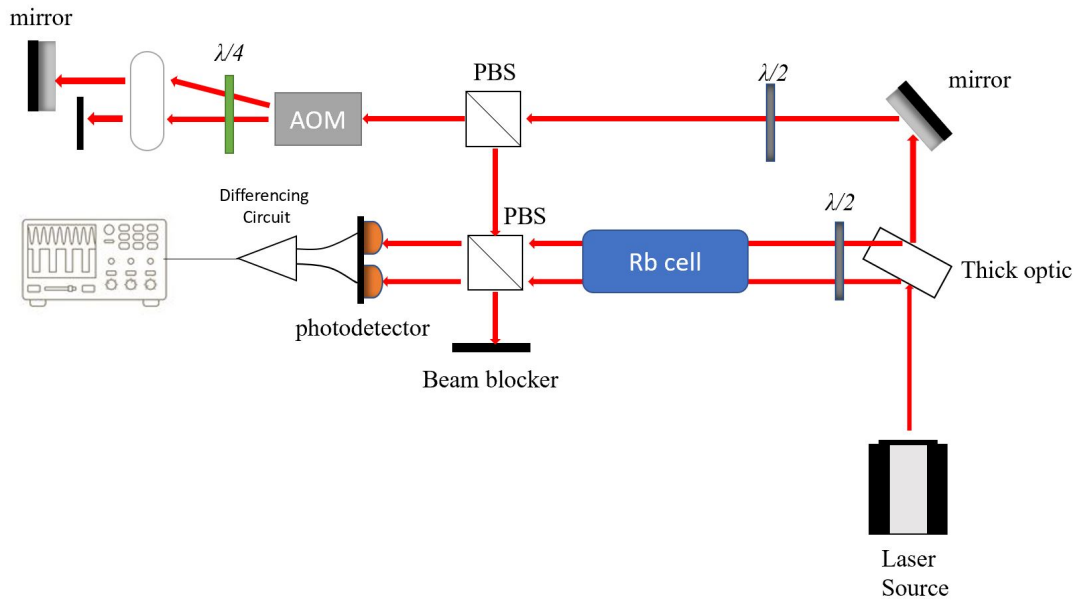


Figure 3.5: This is the diagram of a double pass spectroscopy setup with an added AOM. This AOM is attached to a radio frequency drive and is used to dither the frequency in the pump beam.

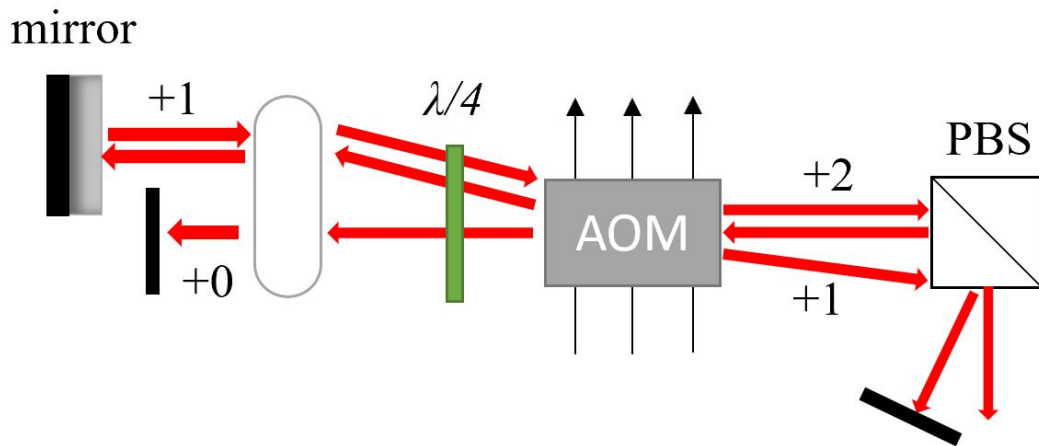


Figure 3.6: A more detailed view of the AOM arm and how the pump beam is reflected in order to achieve double the phase shift while keeping the beam on its original path. The AOM alters the beams phase by the arrows shown behind the AOM in the figure.

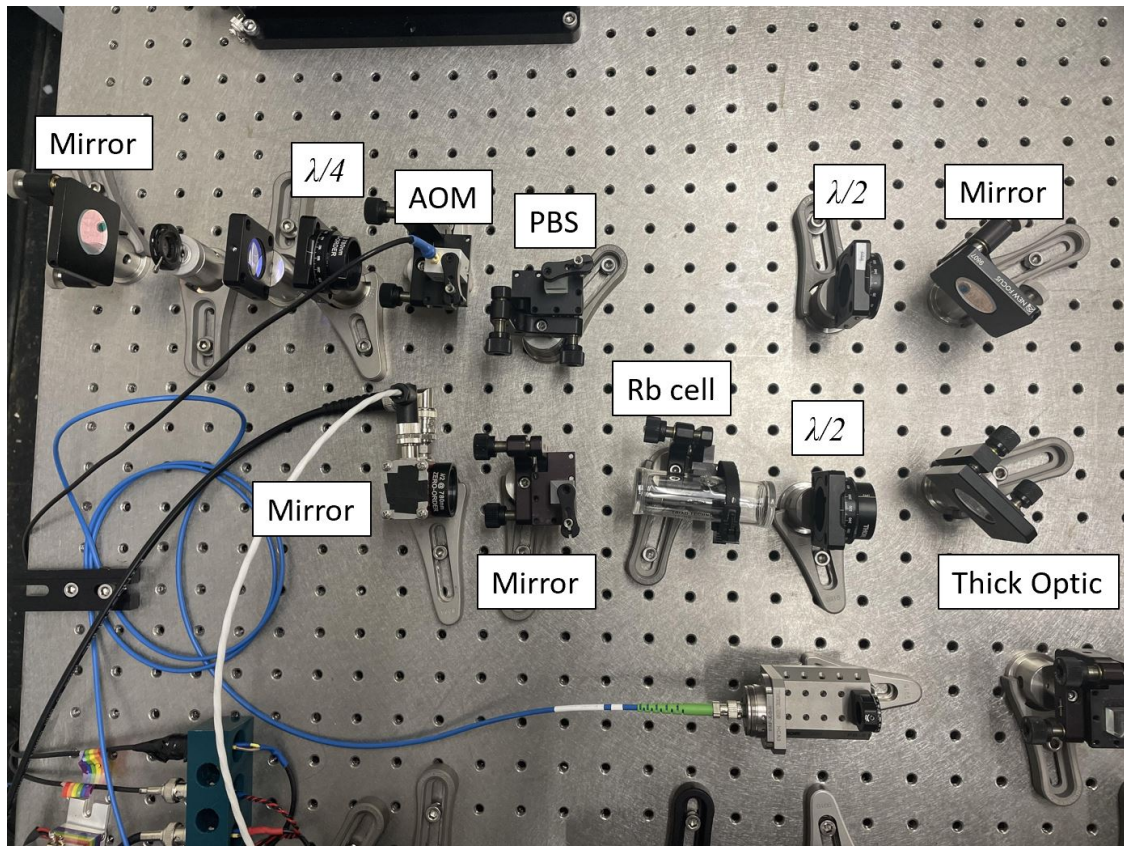


Figure 3.7: The actual setup used in the lab that reflects the diagram in Figure 3.5. Not shown is the laser and optical isolator since multiple experiments are being run with one laser it is reflected into this setup from the bottom of the picture as in the diagram.

When implementing the setup described, there are a few practical applications to consider. The Lock-in amplifier used can be tuned to improve the accuracy of the derivative by decreasing the time constant used. Yet all lock-in amplifiers have a minimum integration time constant ranging from 1 msec up to seconds which limits the possible dither frequency. In order to return the derivative signal, it is necessary for the amplifier to be able to pick up multiple data points within one time constant. Furthermore, the maximum dither frequency from the lock-in amplifier is 100 kHz. We can then assume a minimum of one hundred points are needed by the amplifier to adequately average non-resonant frequencies to zero. With this, we see that the minimum time constant of 1ms results in a feedback bandwidth of 1 kHz.

It is possible to superimpose the saturated absorption spectrum on top of the derivative gained from the lock-in amplifier to see how they align as in Figure 3.8. Ideally the peaks of the original spectrum would be at the zero values of the derivative signal. Yet in the signals observed there is a

notable phase shift between the expected zero values and the peaks. This is due to the integration time constant but is not substantial enough to affect the final lock point.

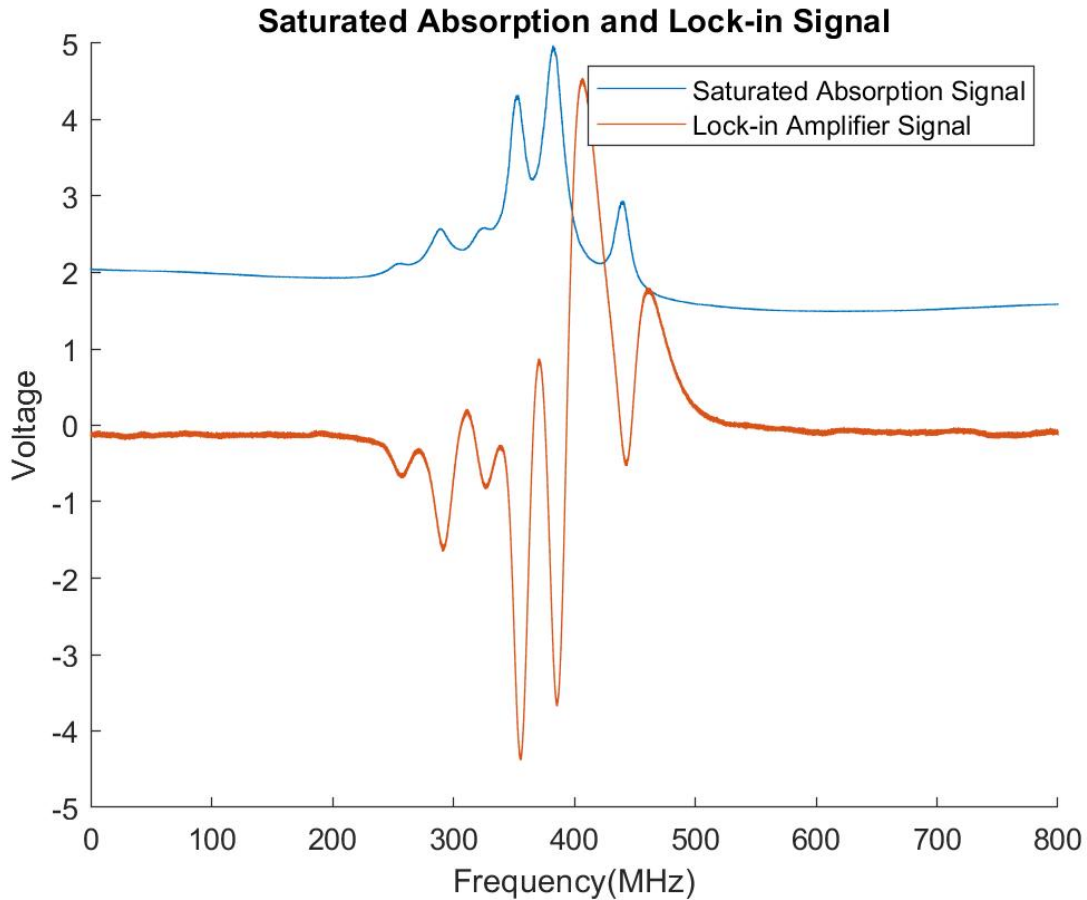


Figure 3.8: The comparison of the signal from the saturated absorption setup and the lock-in amplifier data that should theoretically be its derivative.

Another way of checking the accuracy of the data returned from the lock-in amplifier would be to take the derivative of the signal itself. Since we just took both signals over the same time span, it is possible to take the time derivative of the saturated absorption spectrum and plot it against the lock-in return as in Figure 3.9. While the signals are not exact, when scaled they do exhibit the same shape while still demonstrating the expected phase shift.

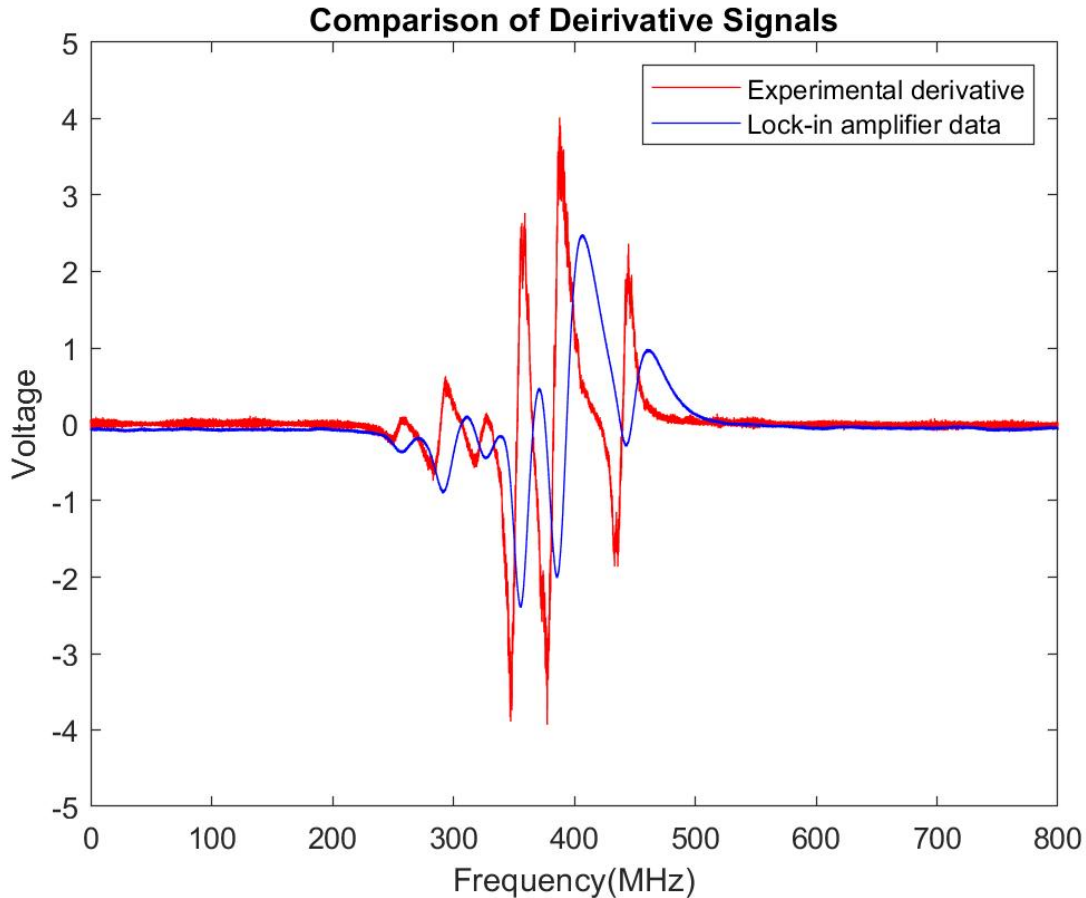


Figure 3.9: The comparison in MATLAB of the derivative returned from the lock-in amplifier and the discrete time derivative of the original signal.

3.3 Increasing the Dither Frequency

The current limitation of 1 kHz for the feedback loop is not high enough for the laboratory goals. While it could work within the lab setup, if an atom interferometer is to leave the lab we would need a much higher feedback frequency. The next step that presents itself for increasing this feedback frequency is increasing the dither frequency of the system. Increasing the dither frequency above the MHz order of magnitude means that certain assumptions made in calculations in the lab previously can no longer be made. As a result, we revisit the atom-laser interaction calculation and deriving a density matrix approach here for a two-level atom, under the action of a modulated pump.

The Hamiltonian of the system including a two level atom is given by

$$\hat{H} = \hbar\omega_0|2\rangle\langle 2| - \hat{\boldsymbol{\mu}} \cdot \mathbf{E}(z, t), \quad (3.8)$$

where

$$\hat{\boldsymbol{\mu}} = \boldsymbol{\mu}_{12}|1\rangle\langle 2| + \boldsymbol{\mu}_{12}^*|2\rangle\langle 1| \text{ and} \quad (3.9a)$$

$$\mathbf{E}(z, t) = \varepsilon_0 \boldsymbol{\epsilon}_L e^{-i\omega_L t - i\Delta\omega \sin(\omega_m t)} + c.c., \quad (3.9b)$$

where $\boldsymbol{\mu}_{12}$ is the transition dipole moment, $\boldsymbol{\epsilon}_L$ is the laser polarization vector, and ε_0 is the field amplitude. The Von Neuman equation of motion for the density operator $\hat{\rho}$ is given by

$$\begin{aligned} \dot{\hat{\rho}} &= -\frac{i}{\hbar} [\hat{H}, \hat{\rho}] \\ &= \frac{i}{\hbar} \left(\hbar\omega_0|2\rangle\langle 2| - (\boldsymbol{\mu}_{12}|1\rangle\langle 2| + \boldsymbol{\mu}_{12}^*|2\rangle\langle 1|)(\varepsilon_0 \boldsymbol{\epsilon}_L e^{-i\omega_L t - i\Delta\omega \sin(\omega_m t)} + c.c.) \right) \rho \\ &\quad - \rho \left(\hbar\omega_0|2\rangle\langle 2| - (\boldsymbol{\mu}_{12}|1\rangle\langle 2| + \boldsymbol{\mu}_{12}^*|2\rangle\langle 1|)(\varepsilon_0 \boldsymbol{\epsilon}_L e^{-i\omega_L t - i\Delta\omega \sin(\omega_m t)} + c.c.) \right). \end{aligned} \quad (3.10)$$

In order to formulate the density matrix we are interested in the matrix

$$\hat{\rho} = \begin{bmatrix} \rho_{11} & \rho_{12} \\ \rho_{21} & \rho_{22} \end{bmatrix} \quad (3.11)$$

where $\rho_{ij} = \langle i|\hat{\rho}|j\rangle$.

Projecting against atomic states and making the rotating wave approximation, we obtain

$$\dot{\rho}_{22} = \frac{i}{\hbar} \left[\boldsymbol{\mu}_{12}^* \rho_{12} \varepsilon_0 \boldsymbol{\epsilon}_L e^{-i\omega_L t - i\Delta\omega \sin(\omega_m t)} - \boldsymbol{\mu}_{12} \rho_{21} \varepsilon_0^* \boldsymbol{\epsilon}_L^* e^{i\omega_L t + i\Delta\omega \sin(\omega_m t)} \right] \quad (3.12a)$$

$$\dot{\rho}_{12} = i\omega_0 \rho_{12} + \frac{i}{\hbar} \left[\boldsymbol{\mu}_{12} (\rho_{22} - \rho_{11}) \varepsilon_0^* \boldsymbol{\epsilon}_L^* e^{i\omega_L t + i\Delta\omega \sin(\omega_m t)} \right]. \quad (3.12b)$$

To change to a frame rotating with the laser frequency, we make the following transformation

$$\rho_{22} = \tilde{\rho}_{22} \quad (3.13a)$$

$$\rho_{12} = \tilde{\rho}_{12} e^{i\omega_L t} \quad (3.13b)$$

and we obtain

$$\dot{\tilde{\rho}}_{22} = \frac{i}{\hbar} \left[\mu_{12}^* \tilde{\rho}_{12} \varepsilon_0 \epsilon_L e^{-i\Delta\omega \sin(\omega_m t)} - \mu_{12} \tilde{\rho}_{21} \varepsilon_0^* \epsilon_L^* e^{i\Delta\omega \sin(\omega_m t)} \right] \quad (3.14a)$$

$$\dot{\tilde{\rho}}_{12} = i [\omega_0 - \omega_l] \tilde{\rho}_{12} + \frac{i}{\hbar} \left[\mu_{12} (\tilde{\rho}_{22} - \tilde{\rho}_{11}) \varepsilon_0^* \epsilon_L^* e^{i\Delta\omega \sin(\omega_m t)} \right]. \quad (3.14b)$$

We know that

$$e^{i\Delta\omega \sin(\omega_m t)} = \sum_{-\infty}^{\infty} J_n(\Delta\omega) e^{in\omega_m t} \quad (3.15)$$

and will make the approximation of using $n = -1, 0, 1$ [19]. Substituting this in we get

$$\dot{\tilde{\rho}}_{22} = \frac{i}{\hbar} \left[\mu_{12}^* \tilde{\rho}_{12} \varepsilon_0 \epsilon_L (J_{-1} e^{i\omega_m t} + J_0 + J_1 e^{-i\omega_m t}) - \mu_{12} \tilde{\rho}_{21} \varepsilon_0^* \epsilon_L^* (J_{-1} e^{-i\omega_m t} + J_0 + J_1 e^{i\omega_m t}) \right] \quad (3.16a)$$

$$\dot{\tilde{\rho}}_{12} = i (\omega_0 - \omega_l) \tilde{\rho}_{12} + \frac{i}{\hbar} \left[\mu_{12} (\tilde{\rho}_{22} - \tilde{\rho}_{11}) \varepsilon_0^* \epsilon_L^* (J_{-1} e^{-i\omega_m t} + J_0 + J_1 e^{i\omega_m t}) \right]. \quad (3.16b)$$

The next step is to define the Rabi frequency, Ω , and the detuning, δ . These quantities are given by

$$\Omega = \frac{2\mu_{12}^* \varepsilon_0 \epsilon_L}{\hbar} \quad \text{and} \quad (3.17)$$

$$\delta = \omega_l - \omega_0. \quad (3.18)$$

We will additionally include incoherent damping phenomenologically in the equations with

$$\dot{\tilde{\rho}}_{22} = -W_{21} \tilde{\rho}_{22} + \frac{i}{2} \left[\Omega \tilde{\rho}_{12} \varepsilon (J_{-1} e^{i\omega_m t} + J_0 + J_1 e^{-i\omega_m t}) - \Omega^* \tilde{\rho}_{21} \varepsilon^* (J_{-1} e^{-i\omega_m t} + J_0 + J_1 e^{i\omega_m t}) \right] \quad (3.19a)$$

$$\dot{\tilde{\rho}}_{12} = -(\gamma_{12} + i\delta) \tilde{\rho}_{12} + \frac{i}{2} \left[\Omega^* (2\tilde{\rho}_{22} - 1) (J_{-1} e^{-i\omega_m t} + J_0 + J_1 e^{i\omega_m t}) \right]. \quad (3.19b)$$

In steady state, the density matrix components will be given by

$$\tilde{\rho}_{12} = a_- e^{-i\omega_m t} + a_0 + a_+ e^{i\omega_m t} \quad (3.20a)$$

$$\tilde{\rho}_{22} = b_- e^{-i\omega_m t} + b_0 + b_+ e^{i\omega_m t}. \quad (3.20b)$$

Substituting this in we get

$$\begin{aligned}
-b_-i\omega_m e^{-i\omega_m t} + b_+i\omega_m e^{i\omega_m t} &= -W_{21}(b_-e^{-i\omega_m t} + b_0 + b_+e^{i\omega_m t}) \\
&+ \frac{i}{2} [\Omega(a_-e^{-i\omega_m t} + a_0 + a_+e^{i\omega_m t})(J_{-1}e^{i\omega_m t} + J_0 + J_1e^{-i\omega_m t}) \\
&- \Omega^*(a_-e^{i\omega_m t} + a_0 + a_+e^{-i\omega_m t})(J_{-1}e^{-i\omega_m t} + J_0 + J_1e^{i\omega_m t})] \quad (3.21a)
\end{aligned}$$

$$\begin{aligned}
-a_-i\omega_m e^{-i\omega_m t} + a_+i\omega_m e^{i\omega_m t} &= -(\gamma_{12} + i\delta)(a_-e^{-i\omega_m t} + a_0 + a_+e^{i\omega_m t}) \\
&+ \frac{i}{2} [\Omega^*(2(b_-e^{-i\omega_m t} + b_0 + b_+e^{i\omega_m t}) - 1)(J_{-1}e^{-i\omega_m t} + J_0 + J_1e^{i\omega_m t})]. \quad (3.21b)
\end{aligned}$$

From this we can derive the following six equations by equating Fourier components

$$b_-(i\omega_m - W_{21}) + a_-\left(\frac{i}{2}\Omega J_0\right) + a_0\left(\frac{i}{2}\Omega J_1 - \frac{i}{2}\Omega^* J_{-1}\right) + a_+\left(-\frac{i}{2}\Omega^* J_0\right) = 0 \quad (3.22a)$$

$$b_0(-W_{21}) + a_-\left(\frac{i}{2}J_{-1}(\Omega - \Omega^*)\right) + a_0\left(\frac{i}{2}J_0(\Omega - \Omega^*)\right) + a_+\left(\frac{i}{2}J_1(\Omega - \Omega^*)\right) = 0 \quad (3.22b)$$

$$b_+(-i\omega_m - W_{21}) + a_-\left(-\frac{i}{2}\Omega^* J_0\right) + a_0\left(\frac{i}{2}\Omega J_{-1} - \frac{i}{2}\Omega^* J_1\right) + a_+\left(\frac{i}{2}\Omega J_0\right) = 0 \quad (3.22c)$$

$$b_-(iJ_0\Omega^*) + b_0(i\Omega^* J_{-1}) + a_-(i\omega_m - (\gamma_{12} + i\delta)) = \frac{i}{2}\Omega^* J_{-1} \quad (3.22d)$$

$$b_-(i\Omega^* J_1) + b_0(i\Omega^* J_0) + b_+(i\Omega^* J_{-1}) + a_0(-(\gamma_{12} + i\delta)) = \frac{i}{2}\Omega^* J_0 \quad (3.22e)$$

$$b_0(i\Omega^* J_1) + b_+(i\Omega^* J_0) + a_+(-i\omega_m - (\gamma_{12} + i\delta)) = \frac{i}{2}\Omega^* J_1. \quad (3.22f)$$

In these six equations we only have six unknowns, yet since the constants can be complex this is not enough information. To solve this, we must take the complex conjugate of the first four equations to allow us to solve for the accurate constants. If done so, we can then form a matrix out of the ten equations. The equations can be made easier to solve numerically by defining a dimensionless time quantity $\tau \equiv \gamma_{12}t$. The resulting equations will look the same except that now, all frequencies (W_{21} , Ω , and ω_m) are now scaled by γ_{12} . In the future this matrix can be used to create a MATLAB code that explicitly solves for the steady state coefficients. This can be compared to the previous steady state solutions of the two-level atom without the modulation in the pump beam. The comparison of these two will allow for the future analysis of the impacts of increasing the dither frequency.

THIS PAGE INTENTIONALLY LEFT BLANK

CHAPTER 4: Results

After developing the new system, it is important to characterize the short and long term behavior. In the short term there was a significant increase in the stability of the laser frequency when just implementing PID control. This can be observed in the standard deviation of Figure 4.1 and how the signal drifts inconsistently. When compared to that of Figure 4.2 which demonstrates noise but also does not show a significant drift when on the same scale. Comparing the two results demonstrates that in the short term there is an added bonus of stability on a small time scale.

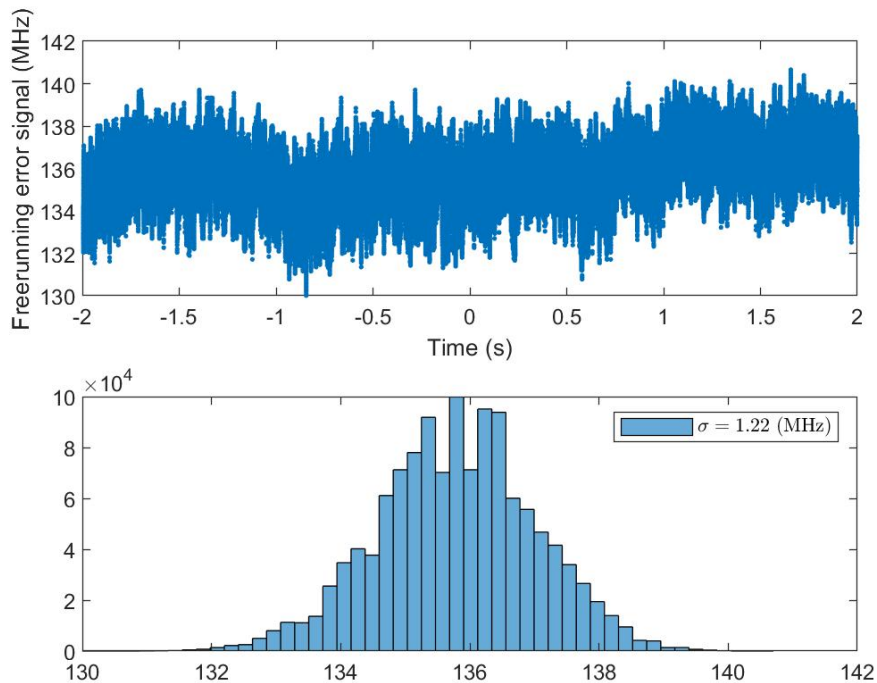


Figure 4.1: An example of what the laser drift looks like over 4 seconds when a control system is not implemented.

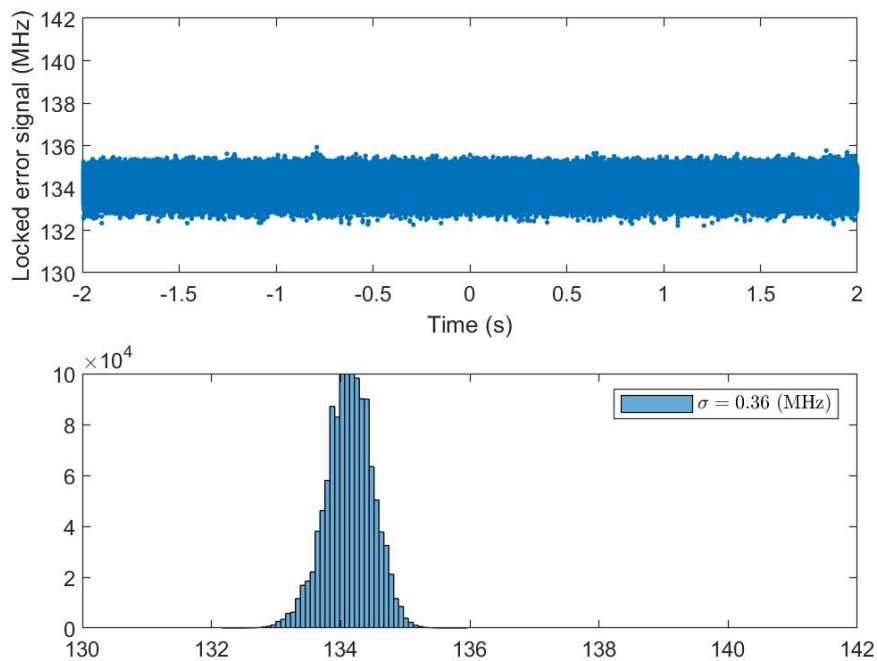


Figure 4.2: An example of what the laser drift looks like over 4 seconds when a PID control system is implemented.

To look at the long term performance of the system, we used a different method of obtaining the data. After implementing the lock-in amplifier it is no longer possible to imply the frequency stability from the output of the PID system. Due to this, we instead measure the frequency of the laser itself by reflecting a portion of the beam before it enters the saturated absorption setup into a device that measures the frequency directly. This data was collected over the course of a day. Once the wavelength data was obtained, we took the Allan variance of it as seen in Figure 4.3. The Allan variance is a mathematical construction that was initially created to study the accuracy of atomic clocks to be able to quantify the accuracy of a clock when there was not a better one with which to compare [20]. It compares the variance of the signal at different averaging values to observe how stable the system is. At the lowest point on the plot, we observe that the lowest variance (and hence error) occurs around 30 seconds, after which the laser begins to drift. This is a value that can be increased in future efforts in order to allow for longer experiments to be conducted without drift.

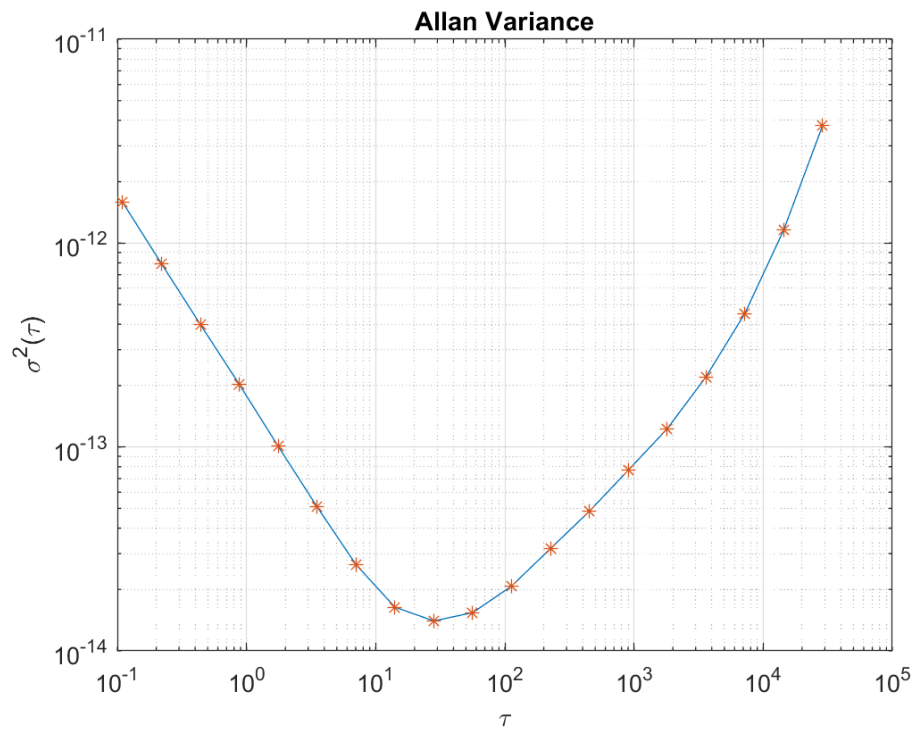


Figure 4.3: The Allan variance plot of when wavelength data from the laser was collected over the course of a day.

THIS PAGE INTENTIONALLY LEFT BLANK

CHAPTER 5: Conclusion

To begin the experiment a basic laser interaction and saturated absorption setup was built that scanned the laser frequency across a range to elicit a response in an atomic cell. After this worked, we modified it in order to achieve a more accurate laser lock.

The first step was to build a double-pass saturated absorption spectroscopy setup that gives a far more accurate version of the transition spectrum of Rubidium than ordinary Doppler spectroscopy. This improvement allowed the observation of the six peaks with three being crossover resonances and the other three being the true transition frequencies.

Once the spectrum had been observed, a PID controller was added to the setup. This allowed us to use the spectrum achieved as the error signal and allowed the frequency to be locked to one of the slopes next to a peak on the spectrum. On the short time scale this dramatically improved the accuracy of the frequency lock of the laser. After this, a lock-in amplifier was added to eliminate noise. When it was used as the error signal, the frequency was then able to be locked at a transition frequency peak.

The theoretical implications of increasing the lock-in amplifier were explored using the density matrix of formulation for the laser-atom interaction. Six equations were found that when paired with their complex conjugates can be used to solve for the steady-state solution of the density matrix. This can be used in the future to explore how high the dither frequency can be pushed while maintaining a lineshape that works for the lab. The higher dither frequency will be critical when building a new lock-in amplifier allowing the lab to push the frequency of the feedback loop higher.

THIS PAGE INTENTIONALLY LEFT BLANK

List of References

- [1] I. Lachow, “The GPS dilemma: Balancing military risks and economic benefits,” in *International Security*, 1995, vol. 20, pp. 126–148.
- [2] R. Christ and R. Wernli, “ROV manual-a user guide for remotely operated vehicles.” [Online]. Available: <https://app.knovel.com/hotlink/toc/id:kpROVMAU03/rov-manual-user-guide/rov-manual-user-guide>
- [3] K. Yu. (2018). *Positioning and Navigation in Complex Environments*. [IGI Global version]. [Online]. Available: <https://www.igi-global.com/gateway/book/181077>
- [4] M. O. Scully and J. P. Dowling, “Quantum-noise limits to matter-wave interferometry,” *Phys. Rev. A*, vol. 48, pp. 3186–3190, Oct 1993. [Online]. Available: <https://link.aps.org/doi/10.1103/PhysRevA.48.3186>
- [5] W. W. Chow, J. Gea-Banacloche, L. M. Pedrotti, V. E. Sanders, W. Schleich, and M. O. Scully, “The ring laser gyro,” *Rev. Mod. Phys.*, vol. 57, pp. 61–104, Jan 1985. [Online]. Available: <https://link.aps.org/doi/10.1103/RevModPhys.57.61>
- [6] V. M. N. Passaro, A. Cuccovillo, L. Vaiani, M. De Carlo, and C. E. Campanella, “Gyroscope technology and applications: A review in the industrial perspective,” *Sensors*, vol. 17, no. 10, 2017. [Online]. Available: <https://www.mdpi.com/1424-8220/17/10/2284>
- [7] O. Carnal and J. Mlynek, “Young’s double-slit experiment with atoms: A simple atom interferometer,” *Phys. Rev. Lett.*, vol. 66, pp. 2689–2692, May 1991. [Online]. Available: <https://link.aps.org/doi/10.1103/PhysRevLett.66.2689>
- [8] K. Bongs, M. Holynski, and J. e. a. Vovrosh, “Taking atom interferometric quantum sensors from the laboratory to real-world applications.” *Nat Rev Phys*, vol. 1, pp. 731–739, 2019.
- [9] W. Demtröder, *Laser Spectroscopy I: Basic Principles*, 5th ed. Springer-Verlag Berlin Heidelberg, 2013.
- [10] W. Heisenberg, “Über den anschaulichen inhalt der quantentheoretischen kinematikund mechanik,” *Zeitschrift für Physik*, vol. 43, no. 3-4, pp. 172–199, Mar 1927. [Online]. Available: <https://doi.org/10.1007/BF01397280>
- [11] S. T. Thornton, *Modern Physics for Scientists and Engineers*, 4th ed. Boston, MA: Brooks/Cole, 2013.
- [12] P. Siddons, C. S. Adams, C. Ge, and I. G. Hughes, “Absolute absorption on rubidium d lines: Comparison between theory and experiment,” *Journal of Physics B: Atomic, Molecular and Optical Physics*, vol. 41, no. 15, p. 155004, Jul 2008. [Online]. Available: <http://dx.doi.org/10.1088/0953-4075/41/15/155004>

- [13] Line width and line shape. [Online]. Available: http://www.pci.tu-bs.de/aggericke/PC4e/Kap_III/Linienbreite.htm. Accessed May 5, 2021.
- [14] D. A. Steck, “Rubidium 85 d line data,” Oregon Center for Optics and Department of Physics, University of Oregon. [Online]. Available: <http://steck.us/alkalidata>
- [15] D. W. Preston, “Doppler-free saturated absorption: Laser spectroscopy,” *American Journal of Physics*, vol. 64, pp. 1432–1436, Nov 1996. [Online]. Available: <https://doi-org.libproxy.nps.edu/10.1119/1.18457>
- [16] T. B. Willy K. Wojsznis. (2013, Mar.). Evolving PID tuning rules. [Online]. Available: <https://www.controleng.com/articles/evolving-pid-tuning-rules/>
- [17] A. Visioli, *Practical PID Control*. London: Springer, 2006.
- [18] *225 Lock-in Amplifier*, Bentham Instruments Ltd, Reading, Berkshire, 2020. [Online]. Available: <http://www.fis.unical.it/files/fl178/8014LockinF225.pdf>
- [19] J. Hall and M. Zhu, “An introduction to phase-stable optical sources,” *Laser Manipulation of Atoms and Ions*, 01 1992.
- [20] D. W. Allan, “Statistics of atomic frequency standards,” *IEEE Proceedings*, vol. 54, pp. 221–230, Feb. 1966.

Initial Distribution List

1. Defense Technical Information Center
Ft. Belvoir, Virginia
2. Dudley Knox Library
Naval Postgraduate School
Monterey, California